HHS Public Access

Author manuscript

Acta Biomater. Author manuscript; available in PMC 2021 July 08.

Published in final edited form as:

Acta Biomater. 2015 September ; 24: 96–105. doi:10.1016/j.actbio.2015.05.036.

Therapeutic intradermal delivery of tumor necrosis factor-alpha antibodies using tip-loaded dissolvable microneedle arrays

Emrullah Korkmaz[1], **Emily E. Friedrich**[2], **Mohamed H. Ramadan**[4], **Geza Erdos**[5], **Alicia R. Mathers**[5,6], **O. Burak Ozdoganlar**[1,2,3], **Newell R. Washburn**[2,4,10], **Louis D. Falo Jr**[5,6,7,8,9,10]

[1]Department of Mechanical Engineering, Carnegie Mellon University, Pittsburgh, Pennsylvania

[2]Department of Biomedical Engineering, Carnegie Mellon University, Pittsburgh, Pennsylvania

[3]Department of Material Science and Engineering, Carnegie Mellon University, Pittsburgh, Pennsylvania

[4]Department of Chemistry, Carnegie Mellon University, Pittsburgh, Pennsylvania

[5]Department of Dermatology, University of Pittsburgh School of Medicine, Pittsburgh, Pennsylvania

[6]Department of Immunology, University of Pittsburgh School of Medicine, Pittsburgh, Pennsylvania

[7]Department of Bioengineering, University of Pittsburgh, Pittsburgh, Pennsylvania

[8]Clinical and Translational Science Institute, University of Pittsburgh School of Medicine, Pittsburgh, Pennsylvania

[9]The University of Pittsburgh Cancer Institute, Pittsburgh, Pennsylvania

[10]The McGowan Institute for Regenerative Medicine, University of Pittsburgh School of Medicine, Pittsburgh, Pennsylvania

Abstract

Tumor necrosis factor-alpha (TNF-α) specific antibodies (anti-TNF-α Ab) have been shown to be potent TNF inhibitors and effective therapeutics for a range of inflammatory diseases. Typically, these drugs are administered systemically, but systemic dosing sufficient to achieve locally effective concentrations in peripheral tissues has been associated with systemic immunosuppression and related adverse events. Here, we evaluated the use of tip-loaded dissolvable microneedle arrays (MNAs) for localized intradermal delivery of anti-TNF-α Ab. MNAs with obelisk shape microneedles that incorporate the antibody cargo in the needle tips were created from carboxymethylcellulose (CMC) using a micromilling/spin-casting fabrication method. We found that Anti-TNF-α Ab integrated into MNAs using this room temperature

Corresponding author: Louis D. Falo, Jr. MD, PhD, Professor and Chairman, Department of Dermatology, University of Pittsburgh School of Medicine, Pittsburgh, PA 15213, lof2@pitt.edu, fax: (412) 864-3734, phone: (412) 864-3760.

fabrication process maintained conformationally dependent TNF-α binding activity. Further, these MNAs efficiently delivered anti-TNF-α antibodies to the dermis of human skin with clinically applicable release profiles. To evaluate MNA delivered anti-TNF-α Ab function, we applied anti-TNF-α Ab containing MNAs to established psoriasiform lesions on the skin of mice. MNA anti-TNF-α Ab treatment reduced key biomarkers of psoriasiform inflammation including epidermal thickness and IL-1β expression. Taken together, these results demonstrate efficient and biologically effective MNA delivery of anti-TNF-α Ab to the intradermal microenvironment of the skin in mice and humans, and support the development of MNA mediated antibody delivery for clinical applications.

Graphical Abstract

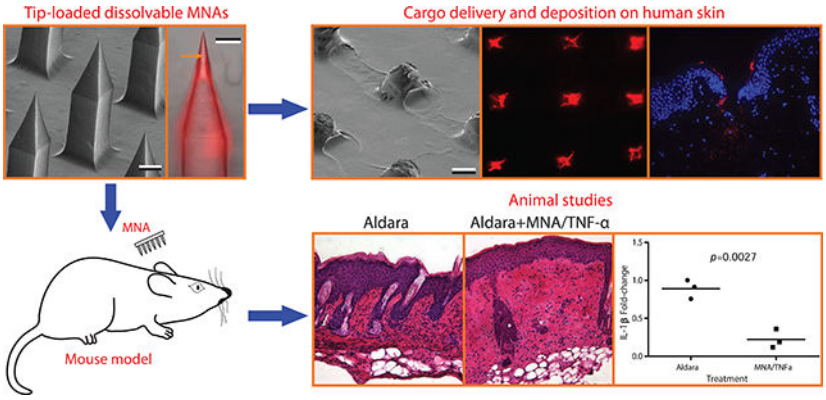

Keywords

Dissolvable microneedle arrays; Intradermal delivery; Tumor necrosis factor-alpha; Therapeutic antibody

1. Introduction

A variety of autoimmune mechanisms result in localized inflammatory skin disease characterized by dysregulated cytokine expression in the cutaneous microenvironment. In particular, localized overexpression of tumor necrosis factor-alpha (TNF-α), a central mediator of inflammation, has been associated with a broad range of autoinflammatory dermatosis and is a rational target for therapeutic inhibition [1–4]. TNF-α specific neutralizing antibodies have been particularly effective in treating inflammatory diseases by selectively binding to soluble TNF-α and thereby reducing TNF-α receptor activation. While subcutaneous and intramuscular injection of TNF-α-blockers have been shown to effectively mitigate skin inflammation, administration of TNF-α inhibitors by these systemic routes requires relatively high doses to achieve locally effective concentrations in the skin [5–9]. These relatively high systemic doses of TNF-α inhibitors can result in non-specific immune suppression that has been associated with increased infection rates and a variety of adverse events [10, 11]. This trade off in efficacy versus off-target immunosuppression limits both efficacy and the broader applicability of TNF-α inhibitors [12].

Topical administration of immunosuppressive agents has considerable advantages over systemic delivery. However, effective topical administration requires penetration of the stratum corneum, the thick outer barrier of the skin, and localization of the therapeutic agent in the intradermal region. Topically applied corticosteroids can be used to effectively treat inflammatory skin diseases. With molecular weights between 200–500 Da, corticosteroids penetrate the stratum corneum which is generally considered to be permissive to molecules of less than 500 Da [13]. However, due to their low molecular weight, corticosteroids have a short residence time in the skin and quickly diffuse into the blood stream. This necessitates repeated applications and frequently long-term use that can lead to undesirable sequelae including loss of skin tone, deterioration of skin cells, and increased risk of infection. On the other hand, antibody therapeutics, typically in the 150 kDa range, are not effective when administered topically as skin penetration is poor due to their high molecular weight. Interestingly, results from topical application of anti-TNF-α Ab in the setting of an already breached skin barrier demonstrate their potential effectiveness if penetration limitations can be overcome. For example, topical application of infliximab was shown to be a promising strategy to improve healing in diabetic skin ulcers [14].

Over the last decade, a number of approaches have been developed for transdermal delivery of therapeutics [15–19]. Most are being developed for transdermal delivery for systemic dosing and are geared towards small molecule drugs and macromolecules smaller than an antibody. Of these techniques, thermal ablation and microneedles have been most successful in the delivery of larger macromolecules. Thermal ablation is a technique in which the skin is heated up to or above 100 °C for microseconds to milliseconds to selectively disrupt the stratum corneum. Thus far, although this technique has demonstrated some success in animal models, general variability in skin thickness and integrity will likely limit the broad application of this technique [17].

Dissolvable microneedle arrays (MNAs) are transdermal delivery systems designed to mechanically penetrate the stratum corneum [20]. A number of micro-fabrication techniques has been developed to create polymer MNAs that can incorporate drug and fully dissolve in skin to deliver therapeutics in a minimally invasive manner [21, 22]. *In vivo* and *in vitro* studies of MNAs loaded with biologics greater than 500 Da supported effectiveness and safety for intradermal drug delivery [23, 24]. Several laboratories, including our own, have demonstrated the use of dissolvable MNAs to deliver vaccines with improved efficiencies, enabling far lower required antigen doses compared to traditional intradermal needle injections [25–27]. We have previously described the use of micromilling/spin-casting technique to develop microneedle arrays with unique microneedle and array geometries designed for precise and specific drug delivery to human skin [27]. The unique advantages of dissolvable polymer MNAs suggest that they could be used to effectively deliver anti-TNF-α Ab intradermally for localized treatment of inflammatory skin disease.

In this paper, we describe the fabrication of MNAs with anti-TNF-α Abs integrated into obelisk-shaped microneedles designed for optimal human skin penetration. Importantly, different from our earlier work where the entire microneedle body and the backing layer was filled with the cargo, in the present work, the fabrication process is modified to integrate the cargo only in the apex (tip) of the obelisk microneedles, enabling efficient, more controlled,

and cost effective drug delivery. These MNAs delivered anti-TNF-α antibodies to the dermis of human skin with clinically applicable release profiles, and anti-TNF-α Ab MNA treatment reduced key indicators of inflammation in a murine model of psoriasiform dermatitis. Taken together, our results support the clinical development of MNA delivered TNF inhibitors for the treatment of localized inflammatory skin diseases.

2. Materials and methods

2.1. Fabrication of tip-loaded dissolvable microneedle arrays

Our previous study demonstrated that dissolvable MNAs with obelisk shape microneedles have considerably better insertion and cargo delivery characteristics than those with traditional microneedle geometries, such as pyramidal microneedles [27]. In this work, the MNA design utilized obelisk microneedle geometry to deliver TNF-α inhibitors. A critical departure from previously demonstrated fabrication approach is that the microneedles of MNAs used in this study are tip loaded with the bioactive cargo (anti-TNF-α Ab) for delivering them to the targeted skin sites. The overall approach used for fabrication of tip-loaded dissolvable MNAs is graphically presented in Fig.1. The approach involves three steps: (a) creation of mastermolds from a wear resistant and easily machinable polymer using the mechanical micromilling process; (b) fabrication of production molds using mastermolds through elastomer molding; and (c) fabrication of tip loaded dissolvable MNAs from production molds using two-step spin-casting technique: (c.1) the sufficient amount of bioactive cargo is loaded into the elastomer mold, and centrifuged at the appropriate temperature and speed into the microneedles. After removal of excess cargo, centrifuging was continued until (only) the tip portions of the microneedles of production molds contain the dry antibody cargo. Next, (c.2) the structural material of MNAs in hyrodgel form is loaded into the elastomer molds, and centrifuged at prescribed temperature and speed until the full density, dry, tip-loaded MNAs are obtained. Currently in our laboratories we are scaled to fabricate 500+ microneedle arrays in a 6 hour day. The fabrication process is readily scalable using industrial grade equipment and automation to dramatically increase output for clinic applications. The fabrication process facilitates easy and rapid changes in geometric and material parameters so that application-specific optimized microneedle array designs can be achieved.

2.1.1. Fabrication of mastermolds and elastomer production molds—

The mastermold geometry, shown in Fig.1, includes four 10×10 MNAs with obelisk geometry microneedles as well as channels that surround each array. The channels are intended to become raised pockets in the production molds to serve as a reservoir for both bioactive cargo and the structural material during the spin-casting process. The width, height, and apex angle of the obelisk shape microneedles were selected to be 210 μm, 700 μm, and 30°, respectively. The tip-to-tip distance of microneedles within an array of 10×10 was 650 μm. A fillet with radius of 35 μm was created at the base of each microneedle, since our previous study has shown that fillets considerably increase the effective strength of the microneedles during insertion [27]. The mastermolds were created from poly (methylmethacrylate) (PMMA, 8560K274, McMaster Carr) using the mechanical micromilling technique performed within a precision miniature machining tool (MMT) using micro-scale cutting

tools. The production molds were then fabricated from a two component clear curable elastomer SYLGARD® 184 polydimethylsiloxane (PDMS, Dow Corning) through elastomer molding enabled by the polymer mastermolds. The elastomer molding is a well-established method presented in the literature for accurate replication [21, 27]. Briefly, the uncured material was mixed with a catalyst at 10:1 SYLGARD®-to-curing agent ratio. Subsequently, the mixture was degassed for 10 min in a vacuum chamber and poured over the mastermold to form an approximately 8 mm layer. This was followed by another step of degassing in the vacuum chamber for 10 min. Next, the mastermold loaded with degassed mixture was placed in an oven, and elastomer was cured at 75 °C for 1 h. The cured PDMS was cooled to room temperature and then separated from the mastermold.

2.1.2. Preparation of anti-TNF-α Ab formulations—Rat anti-mouse TNF-alpha antibody was purchased from AbD serotec. Antibody was labeled with Cy3 fluorescent dye and purified through extensive dialysis against phosphate-buffered saline (PBS). Final product used for MNAs contained 0.5 mg/mL of anti-TNF-α Ab. Penetration enhancer used for comparative study was dimethyl sulfoxide (DMSO). Treatments were prepared by mixing 50% of DMSO with antibody in PBS. Final product used for topical application with penetration enhancer again contained 0.5 mg/mL of anti-TNF-α Ab.

2.1.3. Preparation of dissolvable materials for tip-loaded MNAs—To serve as the structural material of the MNAs, a biocompatible and dissolvable polymer, low viscosity sodium carboxymethyl cellulose (CMC, cat# C5678, Sigma-Aldrich, St Louis, MO) was used. The dry powdered form of CMC was dissolved in deionized (DI) water until the CMC-hydrogel with 20 wt% mass concentration was obtained. The CMC-hydrogel was refrigerated at 4 °C for 24 h to equilibrate, and subsequently centrifuged at 2000g for 30 min to remove the occasional bubbles from the hydrogel prior to creating the CMC-MNAs.

2.1.4. Spin-Casting—Tip-loaded CMC-MNAs with obelisk shape microneedles were fabricated through two-step spin-casting technique using a centrifuge (ThermoFisher Scientific – Heraeus Multifuge X3R with Swinging Bucket Rotor TX 750). First, the tip loading was performed. To this end, 15 μL of antibody cargo was dispensed over each of the PDMS production molds and the production molds were centrifuged for 3 min at 10 °C and at 3500g to fill the obelisk-shaped cavities. Once the production molds were filled completely, the excessive antibody cargo within the reservoir of the production molds was recovered. The production molds were again centrifuged for 30 min at 10 °C and at 3500g to ensure that the dry bioactive cargo is located at the tip portion of the obelisk-shaped cavities in the production molds. After tip loading was successfully achieved, considering the geometry of the production molds, sufficient amount of CMC-hydrogel was loaded over the production molds to fill the obelisk-shaped geometries in the production molds and to form the backing layer of the MNAs. For each tip-loaded MNA, 50 μL of CMC-hydrogel was placed over the each of the production molds. The CMC-hydrogel loaded production molds were then placed in the centrifuge, and centrifuged for 6 h at 10 °C and at 3500g to obtain tip-loaded dissolvable MNAs with above 95% dryness ratio.

2.1.5. Geometric characterization of fabricated MNAs—The geometries of the fabricated mastermolds and tip-loaded CMC-MNAs were observed from environmental scanning electron microscope (ESEM-Quanta 600) and bright light field microscope images. Furthermore, the production molds were imaged using a bright field microscope to investigate tip loading. To better demonstrate the presence of Cy3-labeled-anti-TNF-α Ab at the tip portion of the CMC-MNAs, MNAs were imaged using a Nikon inverted fluorescence microscope equipped with a charge-coupled device (CCD) camera and a Nikon transmission fluorescent microscope.

2.2. The integrity and activity of anti-TNF-α Ab

2.2.1. Anti-TNF-*α* Ab amount in tip-loaded CMC-MNAs—To determine the amount of anti-TNF-α Ab in tip-loaded CMC-MNAs, Rat IgG ELISA kit was purchased from Abcam (Cambridge, England) and used according to the kit instructions. MNAs were dissolved in 0.1 M sodium bicarbonate for 15 s at 0.05 mL/patch and diluted 10x for the assay in assay diluent.

2.2.2. Binding affinity measurements—To test the activity of anti-TNF-α Ab in tip-loaded CMC-MNAs, binding affinity was determined based on methods previously described by our laboratory using the ForteBio Octet QK system, which measures optical thickness of a streptavidin-functionalized sensor tip [28, 29]. Recombinant mouse TNF-alpha (R&D systems Inc, Minneapolis, MN) was biotinylated using EZ link sulfo-NHS-LC-LC-biotin (Thermo Fischer Scientific, Rockville, IL), which binds strongly to the streptavidin tip. Steptavidin sensor tips were hydrated in PBS for at least 5 minutes prior to starting the experiment. The experimental parameters consisted of the following dipping sequence: PBS baseline, 1 min; TNF-α loading, 2 min; biocytin quench (10 μg/mL), 3 min; PBS wash, 3 min; PBS baseline 2, 3 min; antibody association (as fresh antibody or dissolved MNA), 15 min; PBS dissociation, 15 min. The association step used a series of at least 3 dilutions of dissolved MNAs. The association rate constants, dissociation rate constants, and equilibrium dissociation constants were determined by using the Fortebio data analysis program, which calculated these values by generating a line of best-fit for the binding isotherm.

2.3. Topical and MNA-directed intradermal delivery of TNF-α-inhibitors to ex vivo human skin

2.3.1. Preparation of ex vivo human skin explants—Human skin explants used in this study were prepared based on the standard methods previously described [30]. Briefly, *ex vivo* human skin samples were obtained as freshly excised plastic surgery residuals under IRB approval and used according to University of Pittsburgh Medical Center guidelines. Human skin samples were prepared using dermatome to a thickness of approximately 2 mm. The resulting human skin samples were comprised of unaltered epidermis and a thin layer of underlying dermis, and maintained as explants in normal physiological state by culture at an air-fluid interface.

2.3.2. Image analysis of topical and MNA-directed intradermal delivery of TNF-α-inhibitors to human skin explants—To image the intradermal delivery of anti-

TNF-α Ab from tip-loaded, obelisk-shaped dissolvable MNAs to human skin explants, tip-loaded CMC-MNAs encapsulating Cy3-labeled anti-TNF-α Ab were fabricated through the spin-casting technique as described above. Prior to application of MNAs to the human skin explants, they were imaged using ESEM. Subsequently, MNAs were applied to human skin explants using a custom-made spring-loaded applicator. Considering the thickness of the skin samples, the travel distance of the impact head of the applicator was limited to 1.5 mm. After 30 min, MNAs were removed and the final shapes of the dissolved MNAs were imaged by ESEM. The targeted human skin samples were then excised and imaged using a Nikon inverted fluorescence microscope fitted with a CCD camera, at 4x optical magnification to show the pattern of the fluorescent Cy3-labeled deposited microneedle materials into the human skin samples.

For qualitative histological assessment of intradermal delivery of anti-TNF-α Ab from tip-loaded CMC-MNAs to human skin, tip-loaded CMC-MNAs were embedded with Cy3-labeled anti-TNF-α and applied to human skin explants as described above. Similarly, Cy3-labeled anti-TNF-α with DMSO solvent was applied to human skin explants topically to demonstrate that even potent solvents do not help penetrate stratum corneum. Subsequently, the targeted human skin samples were fixed in 2% paraformaldehyde followed by immersion in sucrose solution, with 3 changes of solution over 24 hours. Tissue sections were then flash frozen in optimum cutting temperature (OCT) histology compound, and cyro-sectioned into approximately 10 μm thick cross-sections. The sectioned human skin samples were counter-stained using nuclear DAPI fluorescent dye. The stained sections were then imaged using a Nikon transmission fluorescent microscope to detect the fluorescent microneedle-materials (Cy3-labeled-anti-TNF-α Ab) into the cross-sections of the human skin explants and fluorescent topical-materials at the surface of the stratum corneum.

2.3.3. Quantitative assessment of MNA-directed delivery of TNF-α-inhibitors to ex vivo human skin—

To quantitatively evaluate the intradermal delivery of anti-TNF-α Ab and kinetics of the intradermal delivery from tip-loaded CMC-MNAs to *ex vivo* human skin, tip-loaded CMC-MNAs with embedded Cy3-labeled anti-TNF-α Ab were prepared through the spin-casting technique as described above. Subsequently, MNAs were applied to human skin explants in six replicates for each treatment of 5, 10, 20, and 40 min using a spring-loaded applicator and then removed. The targeted skin areas were sampled using an 8 mm biopsy punch. The deposited Cy3 fluorescence dye was released from the skin samples by ProteaseK digest at 37 °C overnight. The cleared samples were dispensed into 96-well plates in quadruplicates and quantitated by spectro-fluorometry at 540/570 nm excitation and emission wavelength. The kinetics of the intradermal delivery of anti-TNF-α Ab from tip-loaded CMC-MNAs to human skin explants was expressed as the percentage of Cy3-labeled-anti-TNF-α Ab content of the MNAs.

2.4. Animal studies

Female Balb/c mice were purchased from The Jackson Laboratories (Bar Harbor, Maine) and used between the ages of 6 and 12 weeks. Mice were housed under specific-pathogen-free conditions and treated according to the University of Pittsburgh's institutional animal care guidelines. To induce a psoriasiform inflammatory response 62.5 mg of Aldara™ cream

(3M pharmaceuticals) containing 5% imiquimod (wt/wt) was applied to the shaved backs of mice daily for 4 days. On day 1 and 3 mice were treated with CMC-MNAs delivering anti-TNF-α Ab. On day 5 mice were sacrificed and cutaneous tissues were collected for histological analysis and qRT-PCR.

2.5. Real-time quantitative RT-PCR

Total RNA was extracted from ears utilizing TRI-reagent (Molecular Research Center; Cincinnati, OH) and reverse transcribed using the QuantiTect Reverse Transcription Kit (Qiagen; Hilden, Germany) according to manufacturers' instructions. Quantitative real-time PCR was performed utilizing the Taqman Gene Expression Master Mix (Life Technologies) according to manufacturer's instructions with IDT PrimeTime qPCR assays (IDT; Coralville, IA) specific for GusB (endogenous control) and IL-1β. Reactions were run and analyzed on a Step One Plus sequence detection system (Applied Biosystems). Expression levels were normalized based on the $2^{-\Delta\Delta Ct}$ method.

2.6. Cutaneous microscopy

To assess cutaneous histology, cross-sections of mouse ears were prepared and stained as previously described [31]. Briefly, frozen cross-sections were embedded in Tissue-Tek OCT (Miles Laboratories; Elkhart, IN) and snap frozen in pre-chilled methyl-butane (Sigma Aldrich). Cryostat sections (8 μm) were mounted onto slides pre-treated with Vectabond (Vector Laboratories; Burlingame, CA), air-dried, and fixed in 96% EtOH and used for H&E staining. Images were acquired using an Olympus Provis AX-70 microscope system (Olympus; Center Valley, PA) with FluoView 500 software.

2.7. Statistical analysis

Comparison of 2 groups was performed by a 2-tailed Student's T-test. A p value of < 0.05 was considered statistically significant.

3. Results and Discussion

3.1. Fabrication of MNAs with tip-loaded cargo.

Critical parameters influencing the feasibility of MNA delivery include penetration and delivery efficiency. The obelisk needle shape we utilize maximizes the proportion of the needle body that enters the skin. This results in an increase in needle volume delivered to the skin and a higher delivery capacity per unit surface area. For example we have shown that MNAs with obelisk needle geometries deliver 4 times more cargo for the same array configuration and microneedle height than pyramidal needle geometries [27]. We reasoned that further efficiencies could be achieved by optimizing the proportion of drug integrated in the skin penetrating portion of the needle body. Thus, a fabrication method that results in drug localized in the needle apex (or tip) would result in a higher proportion of drug delivery. This efficiency of drug delivery is particularly important when the therapeutic approach requires delivery of a bioactive agent that is rare or expensive, such as an antibody.

Dissolvable MNAs that integrate the antibody cargo primarily in the tip portion of the needles (referred to as "tip-loaded") were fabricated using a three-stage fabrication

technique through mastermold (positive) to production mold (negative) to final dissolvable MNAs (positive). This is schematically depicted in Fig. 1. The mastermolds were created from a PMMA workpiece using the mechanical micromilling process to circumvent the expensive, equipment sensitive, and geometrically limited SU-8 based lithography and laser etching techniques [27]. PMMA was chosen as the mastermold material since it is easy to machine and provides good wear resistance during fabrication of production molds through elastomer molding (Fig. 1A). An ESEM image of an entire fabricated mastermold and a high magnification insert of individual obelisk-shaped microneedles are shown in Fig. 2A. The PMMA mastermolds were then used to fabricate several flexible production molds from PDMS through elastomer molding (Fig. 1B). PDMS was selected as the production mold material due to its flexibility and low cost.

MNAs with tip-loaded anti-TNF-α Abs were fabricated from low viscosity sodium carboxymethyl cellulose (CMC) using PDMS production molds through a two-step spin-casting technique (Fig. 1C). This fabrication process enables room temperature processing throughout, increasing the likelihood that the conformationally dependent bioactivity of the integrated anti-TNF-α Abs would be preserved. Further, CMC was chosen as the structural material for the MNAs because it is a bio-dissolvable, mechanically strong, and water soluble polymer [27, 32]. Further, it can be intradermally injected with no toxic or inflammatory effects, which facilitates repetitive treatments for autoinflammatory diseases with relapsing-remitting nature [33]. Furthermore, the general characteristics of the CMC based-MNAs shown by us and other laboratories support drug stability within the device for a broad range of bioactive cargos, a feature particularly useful for applications to populations with limited resources or disadvantaged socio-economic conditions [34–37]. In the first step, the bioactive cargo was loaded into the elastomer mold and forced into the tips of the microneedle wells by centrifugation. Then, CMC hydrogel was layered into the elastomer molds that were centrifuged again to form an anti-TNF-α Ab integrated CMC tip. Fig. 2B shows top-view (*en face*) and front-view bright light microscope images of the production mold after tip loading, and an image of an individual tip-loaded microneedle cavity. In this image, fluorescent labeling of anti-TNF-α Ab with Cy3 enables visualization of the antibody during the fabrication process, and reveals uniform tip loading visible within the production mold (Fig. 2B). After tip loading, production molds were loaded with 20 wt% CMC hydrogel to both fill the obelisk-shaped microneedle cavities, and to form the backing layer of the MNAs. To avoid formation of voids between layers in the microneedles that could potentially decrease their mechanical strength, low viscosity CMC was used during this portion of the fabrication process. Bright field microscope images of the final tip-loaded MNA demonstrate localization of Cy3-labeled anti-TNF-α Ab in the needle tips, as further demonstrated by the insert showing a single needle from the MNA at high magnification (Fig. 2C). Tip localization of Cy3-labeled anti-TNF-α Ab was confirmed by fluoresence microscopy analysis. MNAs with embedded Cy3-labeled anti-TNF-α Ab were imaged using a Nikon inverted fluorescence microscope fitted with a CCD camera and a Nikon transmission fluorescent microscope. En face views of an intact MNA (Fig. 2D), and high magnification images of individual obelisk-shaped microneedles demonstrate the presence and uniformity of Cy3-labeled anti-TNF-α Ab cargo in the needle tips (Fig. 2E,F).

3.2. Binding affinity of MNA integrated anti-TNF-α Abs.

The ability of anti-TNF-α Abs to specifically bind their TNF-α ligand depends on the integrity of their conformationally dependent antibody binding sites. This tertiary protein structure is relatively unstable and susceptible to changes in temperature, pH, mechanical stress, and other factors. We designed the fabrication process with these limitations in mind, utilizing compatible materials and room temperature processing throughout. To evaluate the specific binding capacity of the MNA integrated anti-TNF-α Abs, MNA microneedles were dissolved in 0.1 M sodium bicarbonate solution and anti-TNF-α Abs quantitated by IgG ELISA. Anti-TNF-α recovered from MNAs and quantified with an IgG ELISA was 1.93 ± .11 μg of the 2 μg loaded per MNA. The purchased ELISA kit was validated to determine if it detected fully intact IgG or if it could also detect denatured and reduced IgG. Less than 1% of the reduced and denatured antibody was detected, which means that 99% of the antibody detected using this ELISA kit is intact, which is important to both MNA loading quantification and proper calibration of binding affinity measurements. Binding affinity of the MNA recovered anti-TNF-α Ab was determined by measuring the optical thickness of a streptavidin-functionalized sensor tip using the ForteBio Octet QK system [26,28], using fresh anti-TNF-α (not MNA integrated) as a positive control. Characteristic association and dissociation curves of TNF-α with anti-TNF-α Ab from anti-TNF-α Ab loaded MNA vs. fresh anti-TNF-α Ab show similar binding characteristics, with differences in apparent thickness attributed to slight differences in antibody concentrations extracted from the MNAs (Fig 3A). Data were normalized to the amount of antibody in each MNA, measured by IgG ELISA. Curves were fit using the ForteBio Octet analysis software and K_D values were averaged for each MNA tested, with a total of 3 MNAs tested per group (Fig 3B). MNA integrated anti-TNF-α Ab demonstrated a similar though marginally decreased binding affinity compared to fresh unintegrated Ab, which had an average K_D of 9.33 ± 3.18 pM, as indicated by the higher average K_D of 50.6 ± .5.84 pM. Our observation that MNA integrated anti-TNF-α Ab maintained picomolar binding affinities supports our hypothesis that these MNAs can deliver functionally active and biologically effective Abs and the feasibility of MNA mediated antibody delivery for clinical applications.

3.3. MNA-directed delivery of anti-TNF-α Abs to human skin.

To investigate delivery characteristics, tip-loaded MNAs carrying integrated Cy3-labeled anti-TNF-α Ab were fabricated as described above. Human skin explants were prepared from freshly excised human skin by methods we previously described [30]. These MNAs were applied to living human skin explants using a spring-loaded applicator, and removed 30 min later. Images of these MNAs before application (Fig 4A) and after removal (Fig 4B) from human skin demonstrate the nearly complete dissolution of the obelisk microneedles extending to the base, and corresponding deposits of Cy3-labeled anti-TNF-α Ab in the targeted skin (Fig 4C). The nearly complete insertion of these microneedles is enabled by the obelisk design that minimizes insertion forces and skin resistance, and improves dissolution characteristics compared to more commonly used alternative needle geometries, thereby enabling increased delivery efficiencies [27].

For skin therapeutics, drug delivery through the stratum corneum and into the epidermal and dermal microenvironments is essential for biologic function. In the case of the MNAs we

have developed, the mechanism of delivery is mechanical penetration of the top layers of the skin, followed by dissolution of the needles in the aqueous environment of the skin. The MNAs are fabricated from bio-dissolvable (water-soluble) materials (polymers) with drug within the microneedle matrix. These needles are strong enough in their dry-state to penetrate the stratum corneum and epidermis, and then rapidly dissolve in the fluid environment of the skin, thereby releasing embedded drug payload.

To anatomically evaluate the delivery of Cy3-labeled anti-TNF-α Ab into human skin, MNAs with integrated Cy3-labeled anti-TNF-α Ab were fabricated and applied to human skin explants as described previously. The targeted human skin was cryosectioned and imaged using a Nikon transmission fluorescent microscope. Histology demonstrates microneedle cavities penetrating through the epidermis into the dermis, and Cy3-labeled anti-TNF-α Ab colocalized throughout the periphery of the microneedle cavity and the cavity base (Fig 4D–F, DAPI nuclear stain, Cy3-labeled anti-TNF-α Ab, and overlay, respectively). In contrast and as expected, Cy3-labeled anti-TNF-α Ab applied with DMSO as a solvent was restricted to the skin surface (Fig 4G–I). These results demonstrate MNA delivery of anti-TNF-α Ab to the epidermis and dermis of human skin.

3.4. Kinetics of MNA-directed anti-TNF-α Ab delivery to human skin.

To evaluate the time-dependent intradermal delivery profile of anti-TNF-α Ab from tip-loaded anti-TNF-α Ab MNAs, MNAs were fabricated with Cy3-labled anti-TNF-α Ab and applied to human skin as described previously, and then removed after the indicated time periods. MNA targeted skin sites were biopsied and transfer efficiency and kinetics of Cy3-labeled anti-TNF-α Ab were determined by measuring Cy3 fluorescence in the target skin samples. The release profile of Cy3-labled anti-TNF-α Ab from tip-loaded dissolvable MNAs is shown in Fig. 5. Within 5 minutes, greater than 50% of the integrated antibody was delivered to the skin. Delivery peaked between 10 and 20 min, with greater than 75% of the MNA integrated antibody delivered to the skin microenvironment.

3.5. MNA-directed anti-TNF-α Ab treatment of psoriasiform dermatitis.

To evaluate the therapeutic potential of MNA delivered anti-TNF-α Ab, we utilized an established murine model of psoriasiform dermatitis [38–40]. In this model, repeated delivery of the TLR7 agonist Aldera induces inflammation that results in immune cell infiltration, KC proliferation and enhanced dermal vascularity [41]. This results in a red, scaly skin phenotype clinically similar to human psoriasis, and shared histologic features including epidermal hyperplasia, inflammatory infiltrates, and increased expression of the proinflammatory mediator IL-1β [38]. Mechanistically, Aldera induces a local shift in the immunoregualtry balance of the skin toward a proinflammatory environment that is associated with psoriatic disease. Localized delivery of immune modifiers has the potential to directly treat autoimmune disease, and to tip the immunoregulatory balance away from a pro-inflammatory environment and toward a more “tolerant” environment. In this way, a locally delivered immune modifier can have direct immediate effects on disease symptoms, in the context of the potential for longer term therapeutic restoration of immune imbalance.

Potent clinical treatments have been developed based on inhibitors of tumor necrosis factor-α (TNF-α), a central mediator of pro-inflammatory responses. Regrettably, efficacy can be limited by off-target side effects of systemically administered TNF-α inhibitors and have included side effects including increased rates of tuberculosis, fungal infections, and lymphoma. By delivering the TNF-alpha inhibitors locally, it may be possible to decrease the total dose administered to the patient, and systemic exposure. This in turn could reduce side effects while, at the same time, increasing the amount of active therapeutic at the site of interest. As such, our approach could potentially provide the basis for effective treatment of many inflammatory diseases by targeting local immune dysfunction.

Briefly, to induce a psoriasiform inflammatory response Aldara™ cream (3M pharmaceuticals) containing 5% imiquimod was applied to the shaved backs of mice daily for 4 days. First, it was confirmed that application of empty MNAs without anti-TNF-α Ab does not have any effect on the Aldara response (data not shown). Next, on day 1 and 3 mice were treated with anti-TNF-α Ab integrated MNAs. Notably in this application the maximum systemic exposure, which would assume that all delivered drug reached the blood, would be approximately 10 fold less than systemic concentrations commonly reached in humans, and another 5,000 fold less in human circulation. On day 5 mice were sacrificed and cutaneous tissues were collected for histological analysis and qRT-PCR. On day 5 a pronounced decrease in psoriasiform inflammation was observed that was characterized by a significant decrease in cellular infiltrates and epidermal thickness at treated sites compared to un-treated control sites. (Fig 6A–C). Moreover, following treatment there was a significant decrease in IL-1β mRNA expression in treated skin compared to untreated skin (Fig 6D). Taken together, these data demonstrate that MNA delivered anti-TNF-α Abs are biologically active and have a therapeutic effect in an animal model of psoriasiform dermatitis.

4. Conclusion

Therapeutic antibodies are being widely developed for the treatment of a broad spectrum of human diseases. Typically these antibodies are administered systemically, requiring high systemic doses to achieve locally effective concentrations. Therapeutically effective systemic dosing can result in off target effects and adverse events that reduce safety and limit optimal dosing/effectiveness and broader applicability. Development of locally targeted delivery strategies has the potential to overcome these limitations, resulting in safer and more effective therapies. This is particularly true for inflammatory skin diseases. The skin has proven to be a formidable barrier to topical antibody delivery.

Here we demonstrate a dissolvable MNA delivery strategy for therapeutic antibodies. Using a unique fabrication process that integrates the antibody cargo into the MNA scaffold while preserving the tertiary protein structure necessary for antibody ligand binding, we show that MNA integrated antibodies have similar binding affinities as non-integrated control antibodies. Further, using MNAs with obelisk-shaped microneedles with optimized insertion and delivery characteristics, and a tip loading strategy that concentrates the antibody cargo in the needle tips to increase delivery efficiency and eliminate waste, we demonstrate efficient delivery of anti-TNF-α Abs to the dermis of human skin with clinically applicable release

profiles. To evaluate the feasibility of MNA antibody delivery for the treatment of inflammatory skin diseases, we sought to intervene in the localized overexpression of tumor necrosis factor-alpha (TNF-α), a central mediator of inflammation that has been associated with a broad range of autoinflammatory skin diseases including psoriasis. Using a mouse model of psoriasiform dermatitis, we demonstrate that MNA delivered anti-TNF-α Ab treatment reduced key biomarkers of psoriasiform inflammation including epidermal thickness and IL-1β expression. Taken together, these results demonstrate efficient and biologically effective MNA delivery of anti-TNF-α Ab to the intradermal microenvironment of the skin in mice and humans, and support the development of MNA mediated antibody delivery for clinical applications.

Acknowledgements

This work was supported by the National Institute of Health Grant R01EB012776. NRW gratefully acknowledges support from the Heinz Endowments (C1747).

References

1. O'Shea JJ, Ma A, Lipsky P. Cytokines and autoimmunity. Nat Rev Immunol 2002;2(1):37–45. [PubMed: 11905836]
2. Hirano T, Kishimoto T. Interleukin-6: possible implications in human diseases. La Ricerca in clinica e in laboratorio 1989;19(1):1–10.
3. Piguet PF, Grau GE, Vassalli P. Tumor necrosis factor and immunopathology. Immunol Res 1991;10(2):122–40. [PubMed: 1717618]
4. Clark IA. How TNF was recognized as a key mechanism of disease. Cytokine Growth F R 2007;18(3–4):335–43.
5. Gottlieb AB, Antoni CE. Treating psoriatic arthritis: how effective are TNF antagonists? Arthritis Res Ther 2004;6(2):31–5.
6. Sfikakis PP. The first decade of biologic TNF antagonists in clinical practice: lessons learned, unresolved issues and future directions. Current Dir Autoimmun 2010;11:180–210.
7. Rozenblit M, Lebwohl M. New biologics for psoriasis and psoriatic arthritis. Dermatol Ther 2009;22(1):56–60. [PubMed: 19222517]
8. Gupta AK, Skinner AR. A review of the use of infliximab to manage cutaneous dermatoses. J Cutan Med Surg 2004;8(2):77–89. [PubMed: 15685387]
9. Paudel KS, Milewski M, Swadley CL, Brogden NK, Ghosh P, Stinchcomb AL. Challenges and opportunities in dermal/transdermal delivery. Ther Deliv 2010;1(1):109–31. [PubMed: 21132122]
10. Scheinfeld N A comprehensive review and evaluation of the side effects of the tumor necrosis factor alpha blockers etanercept, infliximab and adalimumab. J Dermatol Treat 2004;15(5):280–94.
11. Wolfe F, Michaud K. Biologic treatment of rheumatoid arthritis and the risk of malignancy: analyses from a large US observational study. Arthritis Rheum 2007;56(9):2886–95. [PubMed: 17729297]
12. Daugherty AL, Mrsny RJ. Formulation and delivery issues for monoclonal antibody therapeutics. Advanced Drug Deliv Rev 2006;58(5–6):686–706.
13. Yang JA, Kim ES, Kwon JH, Kim H, Shin JH, Yun SH, Choi KY, Hahn SK. Transdermal delivery of hyaluronic acid -- human growth hormone conjugate. Biomaterials 2012;33(25):5947–54. [PubMed: 22632765]
14. Streit M, Beleznay Z, Braathen LR. Topical application of the tumour necrosis factor-alpha antibody infliximab improves healing of chronic wounds. Int Wound J 2006;3(3):171–9. [PubMed: 16984574]
15. Brown MB, Martin GP, Jones SA, Akomeah FK. Dermal and transdermal drug delivery systems: current and future prospects. Drug Deliv 2006;13(3):175–87. [PubMed: 16556569]

16. Ranade VV. Drug delivery systems. 6. Transdermal drug delivery. J Clin Pharmacol 1991;31(5):401–18. [PubMed: 2050824]
17. Levin G, Gershonowitz A, Sacks H, Stern M, Sherman A, Rudaev S, et al. Transdermal delivery of human growth hormone through RF-microchannels. Pharm Res 2005;22(4):550–5. [PubMed: 15846462]
18. Prausnitz MR, Langer R. Transdermal drug delivery. Nat Biotechnol 2008;26(11):1261–8. [PubMed: 18997767]
19. Durand C, Alhammad A, Willett KC. Practical considerations for optimal transdermal drug delivery. Am J Health Syst Pharm 2012;69(2):116–24. [PubMed: 22215357]
20. Arora A, Prausnitz MR, Mitragotri S. Micro-scale devices for transdermal drug delivery. Int J Pharm 2008;364(2):227–36. [PubMed: 18805472]
21. Lee JW, Park JH, Prausnitz MR. Dissolving microneedles for transdermal drug delivery. Biomaterials 2008;29(13):2113–24. [PubMed: 18261792]
22. Donnelly RF, Majithiya R, Singh TR, Morrow DI, Garland MJ, Demir YK, et al. Design, optimization and characterisation of polymeric microneedle arrays prepared by a novel laser-based micromoulding technique. Pharm Res 2011;28(1):41–57. [PubMed: 20490627]
23. Liu S, Jin MN, Quan YS, Kamiyama F, Kusamori K, Katsumi H, et al. Transdermal delivery of relatively high molecular weight drugs using novel self-dissolving microneedle arrays fabricated from hyaluronic acid and their characteristics and safety after application to the skin. Eur J Pharm Biopharm 2014;86(2):267–76. [PubMed: 24120887]
24. Donnelly RF, Raj Singh TR, Woolfson AD. Microneedle-based drug delivery systems: microfabrication, drug delivery, and safety. Drug Deliv 2010;17(4):187–207. [PubMed: 20297904]
25. Hegde NR, Kaveri SV, Bayry J. Recent advances in the administration of vaccines for infectious diseases: microneedles as painless delivery devices for mass vaccination. Drug Discov Today 2011;16(23–24):1061–8. [PubMed: 21782969]
26. Alarcon JB, Hartley AW, Harvey NG, Mikszta JA. Preclinical evaluation of microneedle technology for intradermal delivery of influenza vaccines. Clin Vaccine Immunol 2007;14(4):375–81. [PubMed: 17329444]
27. Bediz B, Korkmaz E, Khilwani R, Donahue C, Erdos G, Falo LD, Jr., et al. Dissolvable microneedle arrays for intradermal delivery of biologics: fabrication and application. Pharm Res 2014;31(1):117–35. [PubMed: 23904139]
28. Sun LT, Bencherif SA, Gilbert TW, Farkas AM, Lotze MT, Washburn NR. Biological activities of cytokine-neutralizing hyaluronic acid-antibody conjugates. Wound Repair Regen 2010;18(3):302–10. [PubMed: 20412551]
29. Sun LT, Buchholz KS, Lotze MT, Washburn NR. Cytokine Binding by Polysaccharide-Antibody Conjugates. Mol Pharmaceut 2010.
30. Morelli AE, Rubin JP, Erdos G, Tkacheva OA, Mathers AR, Zahorchak AF, et al. CD4+ T cell responses elicited by different subsets of human skin migratory dendritic cells. J Immunol 2005;175(12):7905–15. [PubMed: 16339526]
31. Mathers AR, Janelsins BM, Rubin JP, Tkacheva OA, Morelli AE, and AT Larregina. Differential capability of human cutaneous dendritic cell subsets to initiate Th17 responses. J Immunol 2009;182:921–33. [PubMed: 19124735]
32. Nair LS, Laurencin CT. Polymers as biomaterials for tissue engineering and controlled drug delivery. Adv Biochem Eng Biotechnol 2006;102:47–90. [PubMed: 17089786]
33. Falcone SJ, Doerfler AM., Berg RA. Novel Synthetic Dermal Fillers Based on Sodium Carboxymethylcellulose: Comparison with Crosslinked Hyaluronic Acid–Based Dermal Fillers. Dermatol Surg 2007;33:136–143.
34. Erdos G, Donahue C, Zhang J, Gambotto A, Ozdoganlar OB, Falo LD. Dissolvable microneedle arrays enable delivery of live adenovectors to the skin for cutaneous transduction and gene immunization. J Invest Dermtol, 2012, 132:S105–105.
35. Erdos G, Donahue C, Williams M, Ozdoganlar OB, Falo LD. Biodegradable dissolving microneedle arrays effectively deliver antigens and adjuvants to skin DCs for the induction of antigen specific immune responses.. J Immunol, 184:48.12.

36. Kim YC, Park JH, Prausnitz MR. Microneedles for drug and vaccine delivery. Adv Drug Deliv Rev. 2012, 64(14): 1547–1568. [PubMed: 22575858]

37. Sullivan SP, Koutsonanos DG, Martin MdP Lee JG, Zarnitsyn V, Murthy N, Compans RW, Skountzou I, Prausnitz MR. Dissolving Polymer Microneedle Patches for Influenza Vaccination, Nat Med. 2010; 16(8): 915–920. [PubMed: 20639891]

38. Flutter B, Nestle FO. TLRs to cytokines: mechanistic insights from the imiquimod mouse model of psoriasis. Eur J Immunol 2013;43(12):3138–46. [PubMed: 24254490]

39. Sweeney CM, Tobin AM, Kirby B. Innate immunity in the pathogenesis of psoriasis. Arch Dermatol Res 2011;303(10):691–705. [PubMed: 21863252]

40. Van der Fits L, Mourits S, Voerman JS, Kant M, Boon L. Imiquimod-induced psoriasis-like skin inflammation in mice is mediated via the IL-23/IL-17 axis. J Immunol 2009;182: 5836–45. [PubMed: 19380832]

41. Swindell WR1, Johnston A, Carbajal S, Han G, Wohn C, Lu J, Xing X, Nair RP, Voorhees JJ, Elder JT, Wang XJ, Sano S, Prens EP, DiGiovanni J, Pittelkow MR, Ward NL, Gudjonsson JE. Genome-wide expression profiling of five mouse models identifies similarities and differences with human psoriasis. PLoS One. 2011 4 4;6(4):e18266. doi: 10.1371/journal.pone.0018266. [PubMed: 21483750]

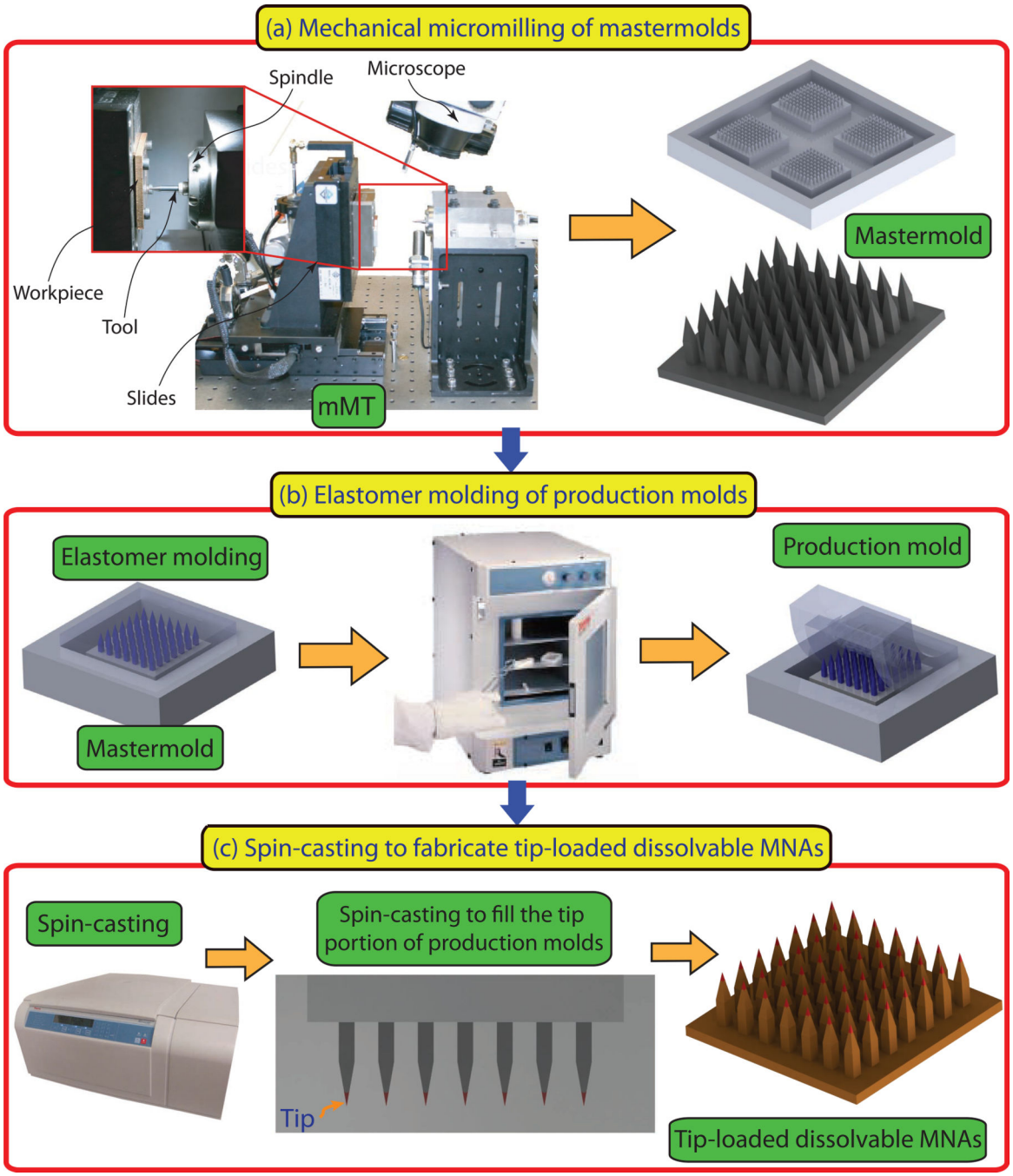

Fig.1.

Description of the micromilling/spin-casting based fabrication approach used for creating tip-loaded dissolvable microneedle arrays. Three-steps: **(a)** Mechanical micromilling of mastermolds. **(b)** Elastomer molding of production molds. **(c)** Spin-casting to localize anti-TNF-α Abs in the apex of obelisk microneedles and fabricate tip-loaded dissolvable MNAs.

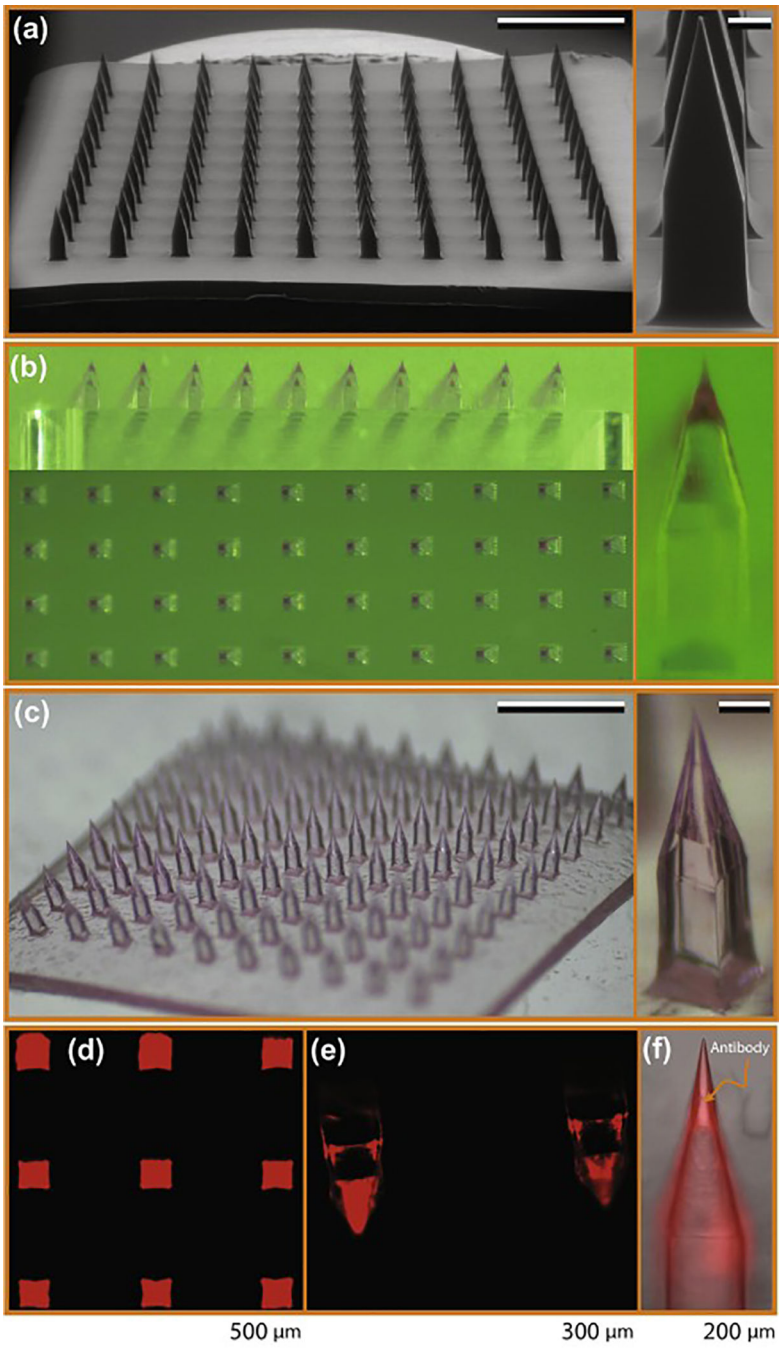

Fig.2.

Tip-loaded dissolvable MNAs created using the micromilling/spin-casting technique for intradermal delivery of anti-TNF-α Abs. **(a)** ESEM images of the PMMA mastermold. Scale bars on the image of array and individual microneedle correspond to 1 mm and 100 μm, respectively. **(b)** Optical microscope images of the production mold after tip loading with bioactive cargo. **(c)** Bright field microscope images of the tip-loaded MNAs. Scale bars on the image of array and individual microneedle correspond to 1 mm and 100 μm, respectively. **(d)** Inverted fluorescence microscope image of a dissolvable MNA tip-loaded with Cy3-

labeled anti-TNF-α Ab. **(e)** Inverted fluorescence microscope image of the individual tip-loaded dissolvable MNAs. **(f)** Merged bright field and fluorescence microscope image of the tip portion of the individual microneedle.

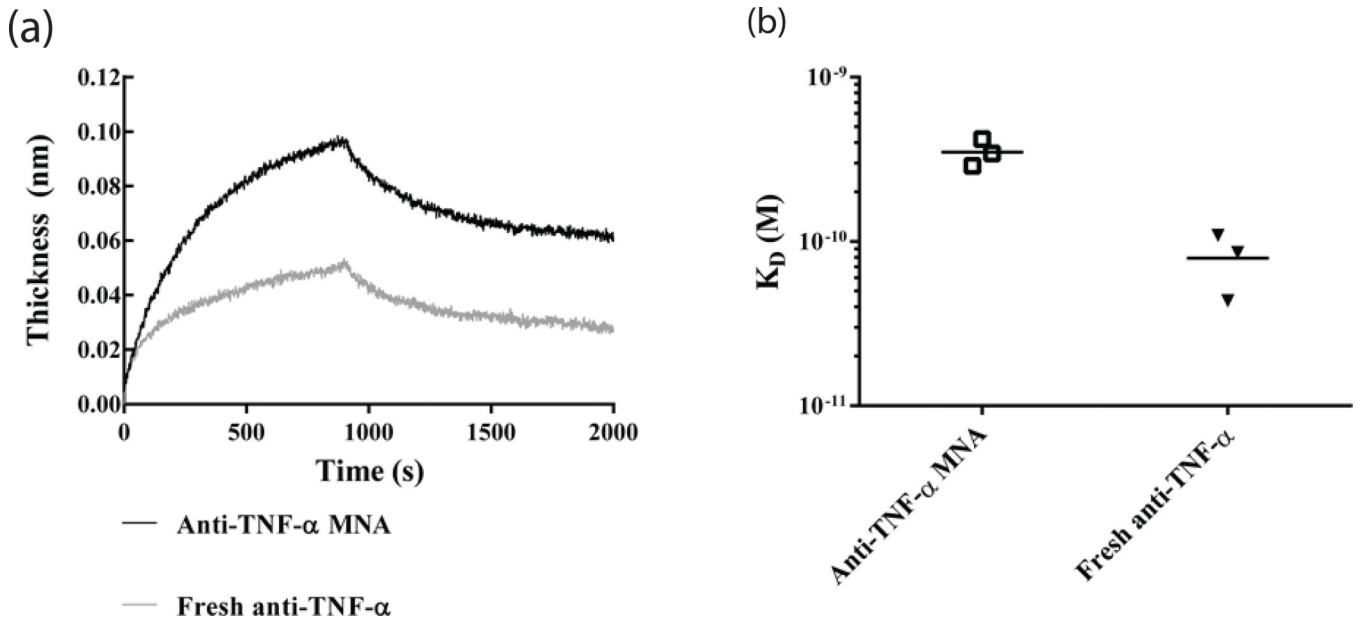

Fig. 3.

TNF-α binding affinity for anti-TNF-α Ab using biolayer interferometry. Biolayer interferometry was used to measure binding affinity of fresh or previously encapsulated anti-TNF-α Ab with TNF-α immobilized on the sensor tip to characterize the effects of processing on antibody binding affinity. **(a)** Characteristic binding curves of fresh and previously encapsulated anti-TNF-α Ab show similar binding kinetics in real time. **(b)** K_D values extracted from binding curves using a 1:1 binding isotherm model show slight increases in K_D for anti-TNF-α Ab previously encapsulated in MNA (K_D = 50.6 ± 5.84 pM) compared to fresh anti-TNF-α Ab (K_D = 9.33 ± 3.18 pM), corresponding to a slight decrease in binding affinity.

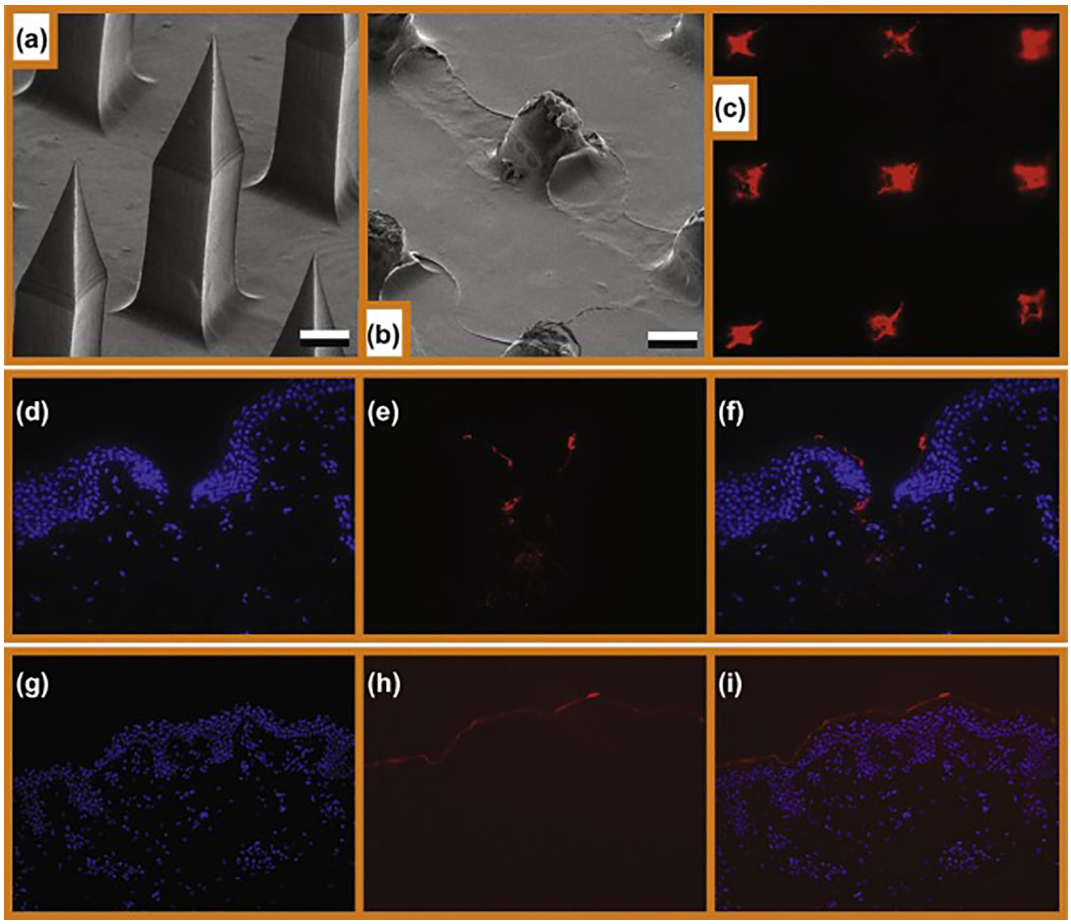

Fig.4.

Microneedle penetration, deposition of cargo and intradermal delivery of anti-TNF-α from tip-loaded CMC-MNAs**. (a)** ESEM image of the microneedle arrays before application. Scale bars correspond to 100 μm. **(b)** ESEM image of the microneedle arrays after 30 min of application. Scale bars correspond to 100 μm. **(c)** Inverted fluorescence microscope image of Cy-3 labeled microneedle traces on living human skin explants. 4 x optical magnification. **(d, e, f)** Intradermal delivery of anti-TNF-α from tip-loaded CMC MNAs. 20x optical magnification. **(g, h, i)** Intradermal delivery of anti-TNF-α from topical application with DMSO. 20x optical magnification.**(d, g)** Fluorescence microscope image of the DAPI stained human skin insertion sites. **(e, h)** Fluorescence microscope images of the Cy3-labeled antibody cargo. **(f, i)** Fluorescence microscope composite images that demonstrate delivery cavities penetrating the epidermis and upper dermis, and delivery of fluorescent cargo of the microneedles.

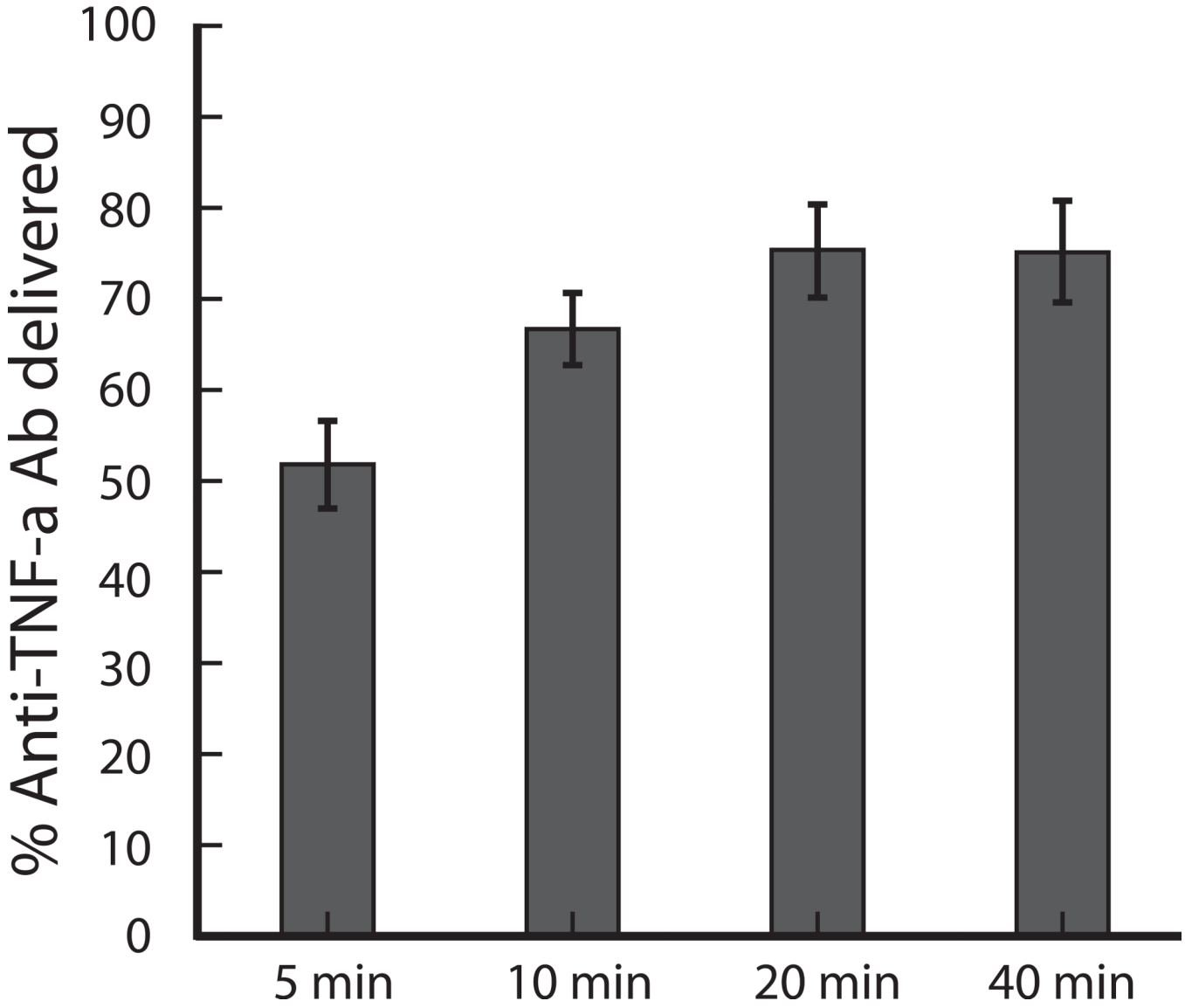

Fig.5.

Intradermal release profiles of anti-TNF-α Ab from tip-loaded CMC-MNAs. Tip-loaded MNAs created as described above were applied to living human skin for the indicated time intervals and then removed. Targeted skin was excised and assayed for Cy3-fluoerescence content by spectrofluorometry. Standard deviation values were from 6 replicates.

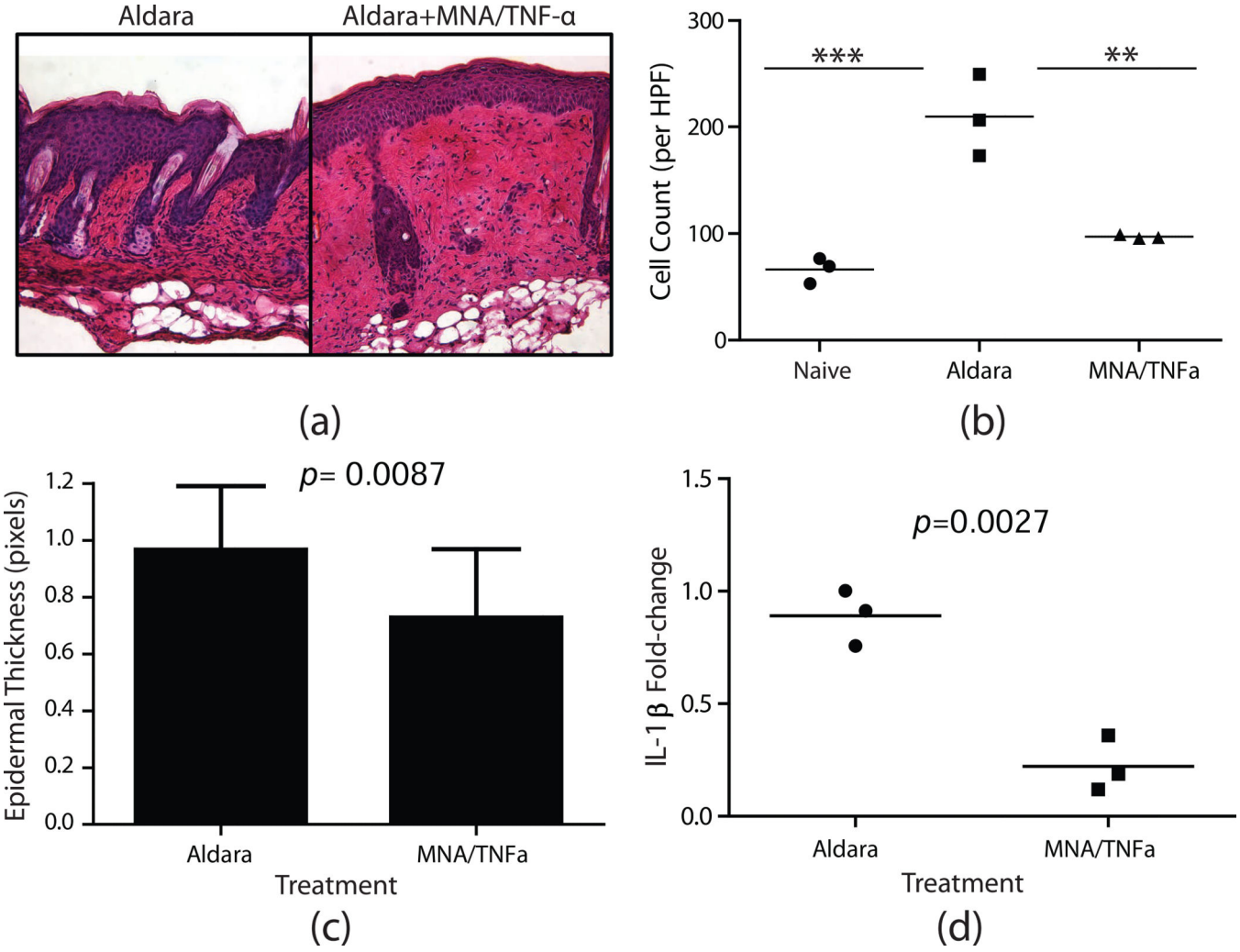

Fig.6.

MNAs delivering TNF-α antibodies abrogate the development of psoriasiform dermatitis. Balb/c mice were treated with Aldara for 4 days. On day 1 and 3 mice were treated with MNA patches delivering TNF-α antibody or Aldara alone as a negative control. **(a)** H&E staining of cutaneous cross-sections collected on day 5. **(b)** Quantitation of cellular infiltrate. Each symbol represents an individual mouse with 10 high-powered fields averaged per mouse. The bar represents the mean of three mice. Asterisks designate a significant difference between indicated treatment groups, ***$p < 0.001$, ** $p < 0.01$. **(c)** Quantitation of epidermal thickness, bars represent the mean thickness of the epidermis from 15 high-powered fields ± S.D. **(d)** Fold-change in IL-1β mRNA expression detected on day 5 by qRT-PCR. Fold-change was determined using the $2^{-\Delta\Delta Ct}$ method in which samples were normalized to GusB endogenous control. Each symbol represents an individual mouse with each sample ran in triplicate. The bar represents the mean of three mice.